OPEN

NPG Asia Materials (2014) 6, e117; doi:10.1038/am.2014.56

www.nature.com/am

ORIGINAL ARTICLE

Bio-inspired porous antenna-like nanocube/nanowire heterostructure as ultra-sensitive cellular interfaces

Biao Kong[1,2], Jing Tang[1], Zhangxiong Wu[2], Cordelia Selomulya[2], Huanting Wang[2], Jing Wei[2], Yongcheng Wang[1], Gengfeng Zheng[1] and Dongyuan Zhao[1,2]

In this study, an unconventional antenna-like heterostructure comprised of arrays of nanoporous Prussian blue (PB) nanocube heads/TiO_2 nanowire (NW) arms (PB-TiO_2) is developed for efficient three-dimensional interfacial sensing of small molecules and cellular activities. Inspired by insect tentacles, which are comprised of both target recognition and signal transduction units, one-dimensional TiO_2 NW arrays are grown, followed by selective growth of nanoporous PB nanocubes on the tips of the NW arrays. Due to their high selectivity and bioaffinity toward cells, long biostability under a cell culture adhesion condition (up to 108 h) is obtained, and with its inherent bio-mimetic enzymatic activity, the obtained nanoporous PB nanocubes (head segment) serve as robust substrates for site-selective cell adhesion and culture, which allows for sensitive detection of H_2O_2. Simultaneously, the single-crystalline TiO_2 NWs (arm segment) provide efficient charge transport for electrode substrates. Compared with PB-functionalized planar electrochemical interfaces, the PB-TiO_2 antenna NW biointerfaces exhibit a substantial enhancement in electrocatalytic activity and sensitivity for H_2O_2, which includes a low detection limit ($\sim$20 nM), broad detection range (10^{-8} to 10^{-5} M), short response time ($\sim$5 s) and long-term biocatalytic activity (up to 6 months). The direct cultivation of HeLa cells is demonstrated on the PB-TiO_2 antenna NW arrays, which are capable of sensitive electrochemical recording of cellular activity in real time, where the results suggest the uniqueness of the biomimic PB-TiO_2 antenna NWs for efficient cellular interfacing and molecular recognition.
NPG Asia Materials (2014) **6,** e117; doi:10.1038/am.2014.56; published online 1 August 2014

INTRODUCTION

Tentacles, which are the long, functional antennas of insects, provide unique and sensitive signal detection capabilities, such as olfaction, gestation and touching, which can guide the motion and functions of insects.[1] The tip of a tentacle, known as the flagellum, is covered with ultra-sensitive olfaction sensing units that can detect specific molecular targets at extremely low concentrations (as low as several molecules per liter). The signal is then transferred through the trunk segment of the tentacle to the neuron networks.[2] This dual-functional antenna structure of the insect tentacles demonstrates a unique modality for signal capture and transduction and could inspire new electrochemical sensor designs for enhanced sensitivity and performance.[3] In particular, a heterostructure comprised of an ultra-sensitive redox unit and a rapid charge transport unit could substantially expand the capabilities of positioning and targeting of cell patterning and in detecting fluctuations and functions of target molecules at an unprecedented level.

Numerous cellular functions are closely correlated with small molecules, such as O_2,[4] glucose,[5] glutathione,[6] NO,[7] CO[8] and H_2O_2,[9] for enzymatic co-factors, signaling and expression. Among them, H_2O_2 is an important reactive oxygen species that can diffuse across cell membranes and lead to oxidative protein modification.[10] Prussian blue (PB) is known as an artificial enzyme peroxidase with porous frameworks, which can efficiently reduce H_2O_2 at extremely rapid catalytic rates with low overpotentials.[11] For example, molecularly imprinted PB films[12] and PB/carbon nanotubes[13] have been used for biosensing because their low overpotentials can exclude interferences from coexisting substances, such as ascorbic acid (AA), uric acid and glucose. However, previous work predominantly used PB nanocrystals that had been post-modified on flat substrates, and thus, only a limited number of crystal faces were exposed to electrolytes, which resulted in lower electrochemical responses. In addition, a relatively large background current still existed due to the secondary electrochemical reactions that occurred on the planar electrode surface.[14] Although bio-mimetic enzyme-based electrical sensors are attractive tools, their use on a robust lab-on-a-chip platform with fast, sensitive and stable three-dimensional (3D) porous interfaces for localized real-time, long-term monitoring of cellular activities and physicochemical changes have not been demonstrated.[15–19]

Inspired by insect tentacles, herein, we developed an unconventional antenna-like heterostructure based on direct growth of porous

[1]Laboratory of Advanced Materials, Department of Chemistry, Shanghai Key Laboratory of Molecular Catalysis and Innovative Materials, Fudan University, Shanghai, China and [2]Department of Chemical Engineering, Monash University, Clayton, Victoria, Australia
Correspondence: Professor G Zheng or Professor D Zhao, Laboratory of Advanced Materials, Department of Chemistry, Shanghai Key Laboratory of Molecular Catalysis and Innovative Materials, Fudan University, Shanghai 200433, China.
E-mail: gfzheng@fudan.edu.cn or dyzhao@fudan.edu.cn
Received 5 January 2014; revised 5 April 2014; accepted 18 May 2014

PB nanocube heads on the tips of TiO_2 nanowire (NW) arms, which can be used for 3D interface recognition and biosensing. Single-crystalline TiO_2 NWs are first hydrothermally grown on conducting substrates, followed by the direct growth of nanoporous PB nanocubes on the tips of the TiO_2 NW arrays via an etching and seed-assisted process (Figure 1, Supplementary Figure S1). The PB nanocubes (head segment) provide site-selective cell adhesion and growth, a large surface area for catalysis and a high sensitivity and selectivity for H_2O_2. The semiconductor TiO_2 NW arms offer fast charge transport from the PB redox centers to the underlying electrode surface due to the excellent electron mobility of TiO_2, the continuous one-dimensional charge transport channels[20,21] and the low background electrical current noise. As a proof-of-concept design, the bio-mimetic PB/TiO_2 antenna NW heterostructures exhibit high selectivity and bioaffinity toward living cells and excellent biostability under cell culture adhesion conditions (up to 108 h). Compared with that of PB-functionalized planar electrochemical interfaces, the electrocatalytic activity on H_2O_2 produced by HeLa cells is enhanced by ~550 times on the PB-TiO_2 antenna NWs, which exhibits a high sensitivity of ~20 nM, broad detection range from 10^{-8} to 10^{-5} M and a fast response time that is within 5 s.

MATERIALS AND METHODS

Materials

AA, dopamine, uric acid and Phorbol 12-myristate-3-acetate (PMA) were purchased from Sigma Chemical Co. (St Louis, MO, USA). Tetrabutyl titanate, hydrochloric acid (37 wt%), $K_4Fe(CN)_6 \cdot 3H_2O$, $K_3[Fe(CN)_6] \cdot 3H_2O$, $NaNO_2$, Na_2SO_3 and H_2O_2 were purchased from Sinopharm Chemical Reagent Co., Ltd. (Shanghai, China). Dulbecco's Modified Eagle's medium (high glucose), RPMI-1640, fetal calf serum, penicillin G, streptomycin and trypsinase were purchased from GIBCO BRL (Grand Island, NY, USA). The fluorine-doped tin oxide-coated glass ~14 Ω per square substrates was purchased from Wuhan Ge-ao Ltd. (Wuhan, China). Other reagents were of analytical grade and used as purchased. All the solutions were prepared by Milli-Q water (Merck KGaA, Darmstadt, Germany) and deaerated with high-purity nitrogen before experiments.

Methods

The PB-TiO_2 NWs were prepared by a two-step interfacial growth method. TiO_2 NWs were first grown on the fluorine-doped tin oxide-coated glass (~14 Ω per square substrates, Wuhan Ge-ao Ltd.) by a hydrothermal method, as described previously.[22,23] Then, the TiO_2 NWs glass substrates were placed within a 125-ml glass bottle, containing 80 ml of HCL (0.005 M) and 136 mg of $K_3[Fe(CN)_6] \cdot 3H_2O$, and stirred for 30 min. The bottle was placed in an oven at 85 °C for 24 h to form the PB nanocrystal seeds. The TiO_2 NWs with PB seeds were washed with neat ethanol and water thoroughly to remove the adsorbed nanocrystals on the TiO_2 NWs surface. To form the PB hierarchical structure on TiO_2 NWs, $K_4Fe(CN)_6 \cdot 3H_2O$ (125 mg) was first added to a HCl solution (0.05 M, 80 ml) under stirring for 30 min. Then, the TiO_2-PB seeds substrate was slowly immersed into the above mixture. After that, the container was placed into an oven and heated at 85 °C for 6–18 h. The obtained PB-armed TiO_2 NWs was taken from the container, washed with deionized water and dried in a vacuum oven at 70 °C for 12 h.

RESULTS AND DISCUSSION

Fabrication of PB-TiO_2 antenna NW heterostructures

The controlled synthesis of the PB-TiO_2 antenna NW heterostructures is performed in two steps. One-dimensional TiO_2 NWs are first hydrothermally grown on fluorine-doped tin oxide substrates, followed by a seed-induced growth of PB nanocubes on the tips of the pre-formed TiO_2 NWs (Experimental section in the Supplementary Information). Scanning electron microscopy images show that the diameters and densities of the TiO_2 NW arrays are well tuned by the acidity of the precursor solution.[22,23] Increasing the solution acidity

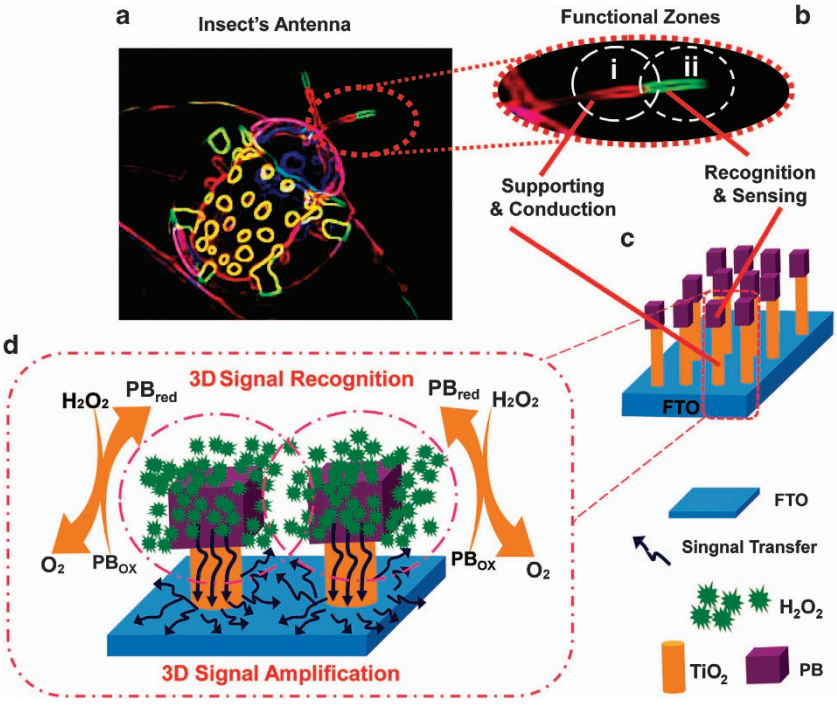

Figure 1 Schematic illustration of three-dimensional (3D) signal recognition and amplification based on porous bio-mimetic antenna nanowire arrays. (**a**) A typical drawing of an insect's antennas according to their different functional zones. (**b**) Enlarged drawing of an antenna with (i) supporting and conduction and (ii) recognition and sensing zones. (**c**) Designed nanoporous bio-mimetic antenna arrays growth on a conducting substrate. (**d**) 3D signal recognition and amplification based on the nanoporous bio-mimetic antenna arrays.

leads to a decrease in both diameter and density (Figure 2a, Supplementary Figures S2a and c). Subsequently, the tips of the TiO_2 NWs are etched using diluted HCL, followed by hydrothermal growth of PB nanocubes (Supplementary Figure S1).[24] At low TiO_2 NW densities, each NW tip is covered with a cluster of nanocubes, which substantially exceed the diameter of the corresponding NW arms (Supplementary Figure S2b). At intermediate NW densities, the measured average diameter and interspacing between adjacent NWs are ~100 and 150 nm, respectively (Figure 2a). The nanocubes with well-defined shapes are grown from each TiO_2 NW (Figure 2b, Supplementary Figure S3). Cross-sectional scanning electron microscopy images also clearly show the bio-mimetic antenna-like heterostructure formation (Figures 2c and d). Compared with bare TiO_2 NWs, the NW tips are covered by a thin layer of PB nanocubes. The edge length of the nanocubes is calculated to be ~150 nm, which is similar to the average interspacing between adjacent TiO_2 NWs. The top-view and side-view transmission electron microscopy (TEM) images show that the number of nanocubes and underlying TiO_2 NWs are similar, which suggests that essentially, each NW tip serves as a growth base for individual nanocubes (Figures 2e and f). This structure provides sufficient space surrounding the crystallized PB nanocubes while maintaining a close contact between the PB nanocubes with the TiO_2 NW bases. When the diameter and density of the TiO_2 NWs are further increased, the interspacing between adjacent NWs is less than the average NW diameter. Thus, the nanocubes on the NW tips accumulate, which forms a multi-layered nanocube assembly (Supplementary Figure S2d). The heterostructure of the PB nanocube head/TiO_2 NW arm is revealed by TEM (Figure 2g, Supplementary Figure S4). The single TiO_2 NWs (Figures 2h and i) and single PB nanocubes (Figures 2j and k) in the heterostructures are further characterized by high-resolution TEM (HRTEM). Both the HRTEM and selected area electron diffraction pattern (Figure 2l) demonstrate the crystallized characteristics of the TiO_2 NWs and PB nanocrystals.

The crystal structure of the PB-TiO_2 antenna NW heterostructures is further examined by X-ray diffraction, which shows a combination of the diffraction peaks of TiO_2 and PB (Figure 3a). No additional peaks other than those of fluorine-doped tin oxide substrates are observed, which indicates the high purity of the samples. Compared with pristine TiO_2 NWs that have negligible absorption in the visible range, the ultraviolet–visible spectra of the PB-TiO_2 antenna NWs show a substantial absorption increase in the range of 500 −900 nm with a maximum at 714 nm, which corresponds to the inter-metal charge transfer bands from Fe^{2+} to Fe^{3+} in PB nanocrystals (Figure 3b).[25] The corresponding energy dispersive X-ray analysis of the PB-TiO_2 NWs shows clear Fe and Ti signals (Supplementary Figure S5). The growth of PB-TiO_2 antenna NWs is further demonstrated by the infrared spectra. In addition to the infrared absorption of pristine TiO_2 NWs centered at 3428 and 1628 cm^{-1}, a new absorption band at 2095 cm^{-1} is observed for the PB-TiO_2 antenna NWs, which corresponds to the C≡N stretching mode in the $Fe^{II}(C{\equiv}N)/Fe^{III}$ pair of PB nanocrystals (Figure 3c).[26] Furthermore, the Raman spectrum of the PB-TiO_2 antenna NWs shows the characteristic band of PB at 2157 cm^{-1}, which further confirms the successful incorporation of PB over TiO_2 NWs (Figure 3d).[13]

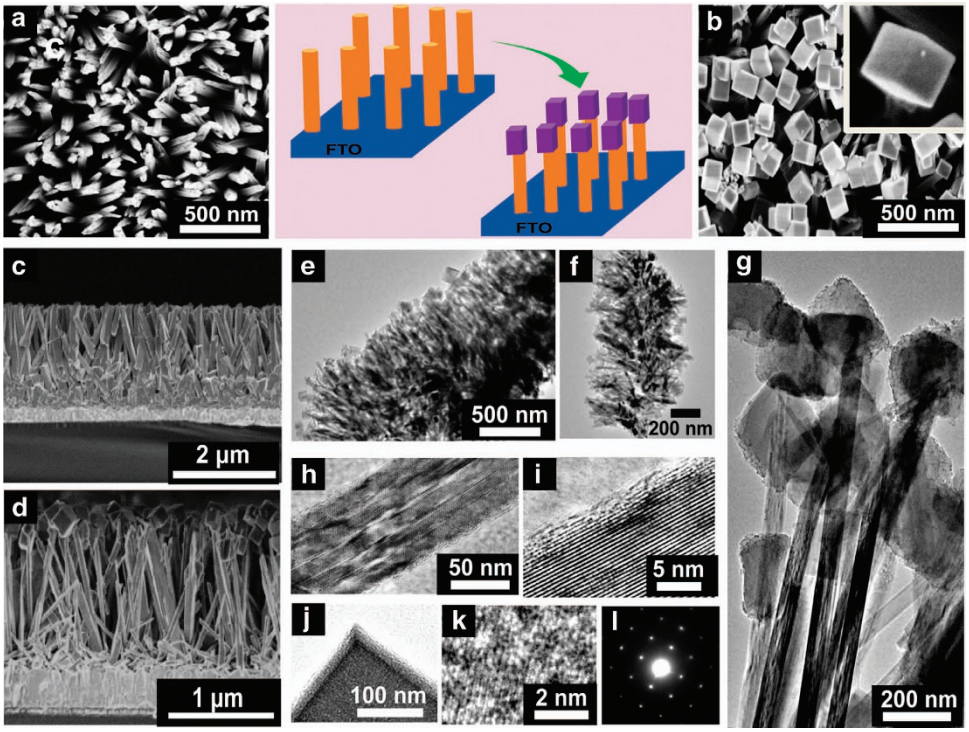

Figure 2 Synthesis and characterization of bio-mimetic antenna Prussian blue (PB)-TiO_2 heterostructure arrays. (**a**) Top-view scanning electron microscopy (SEM) images of the TiO_2 nanowire (NW) arrays on fluorine-doped tin oxide (FTO)-coated glass substrates at an intermediate density. (**b**) Top-view SEM images of PB-TiO_2 NWs at an intermediate density via an etching and seed growth method. (**c**,**d**) Side-view SEM images of (**k**) TiO_2 NW arrays and (**l**) PB-TiO_2 NW arrays at an intermediate density. (**e**) Side-view, (**f**) top-view and (**g**) enlarged transmission electron microscopy (TEM) images of synthesized PB-TiO_2 NW arrays at an intermediate density, as in **e**. (**h**,**i**) High-resolution TEM (HRTEM) and enlarged HRTEM image of a single TiO_2 NW. (**j**,**k**) HRTEM and enlarged HRTEM image of a single PB nanocube. (**l**) Selected area electron diffraction (SAED) pattern of a single PB nanocube.

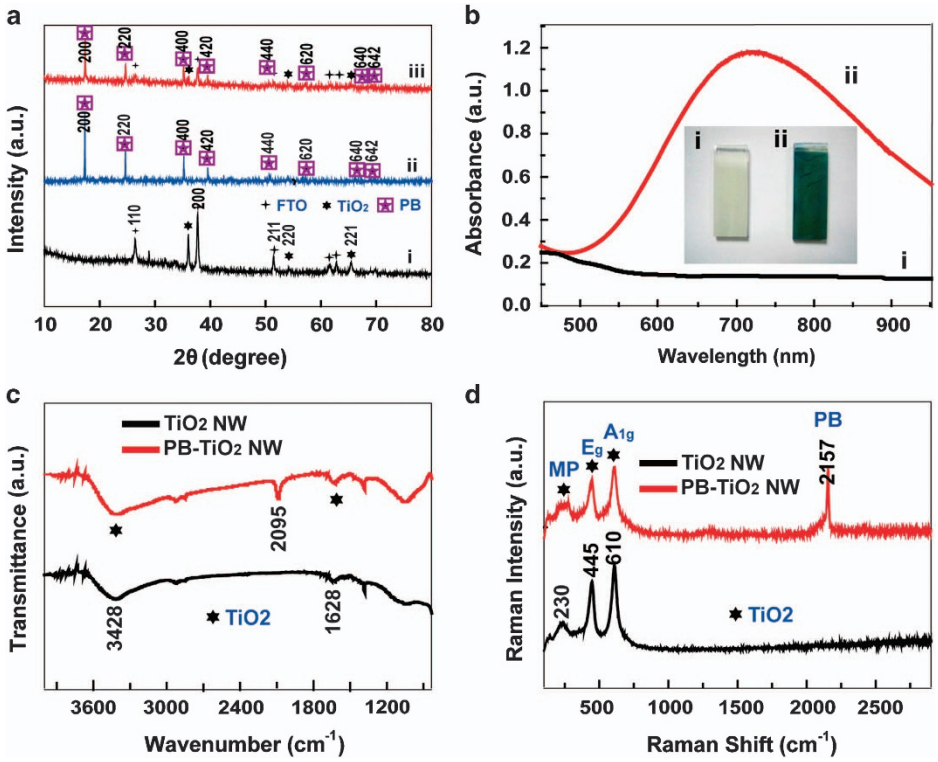

Figure 3 (**a**) X-ray diffraction spectrum of TiO_2 nanowires (NWs), Prussian blue (PB) nanocraystals and PB-TiO_2 NWs.The peaks of PB, blank TiO_2 and fluorine-doped tin oxide substrates are marked. (**b**) The ultraviolet–visible diffused reflectance spectrums of blank TiO_2 NWs and PB-TiO_2 NWs. Inset: the corresponding images of blank TiO_2 NWs and PB-TiO_2 NWs. (**c**) Fourier transform infrared spectroscopy spectra of the TiO_2 NWs (black curve) and PB-TiO_2 NWs (red curve). (**d**) Raman shift spectra of TiO_2 NWs (black curve) and PB-TiO_2 NWs (red curve).

The synthesis mechanism of the proposed etching and seed-assisted process is as follows. First, the intermediate PB seed-modified TiO_2 NWs are observed on the tips of pristine TiO_2 NWs, in which the composite TiO_2 NWs have identical close-packed cubic structures (Supplementary Figure S6). Thus, no clear phase separation occurs on the TiO_2 NW interfaces during the hydrothermal growth process. The removal of PB nanocrystals by an alkaline solution at room temperature for 5 h from the PB-TiO_2 NWs increased the porous property on the top of the TiO_2 NWs (Supplementary Figure S7), which suggests the existence of acid etching during the hydrothermal process. For comparison, the growth without PB seeds does not result in any nanocube structures on the tips of the TiO_2 NWs (Supplementary Figure S8). However, the growth with acid etching only and in the absence of seeds shows that no nanocube clusters formed on the TiO_2 NWs during the hydrothermal process (Supplementary Figure S9); only sporadic PB nanocrystals are adsorbed on the surface of the TiO_2 NWs.

Electrochemical performance

The electrochemical properties of the PB-TiO_2 antenna NW heterostructure are investigated by the cyclic voltammetry method. For comparison, the pristine TiO_2 NWs are also measured under similar conditions. No redox peaks except for the capacitive current are observed for the pristine TiO_2 NW electrode, whereas the PB-TiO_2 antenna NW electrode has a pair of redox peaks at 0.23 and 0.18 V (Figure 4a), which corresponds to the reversible conversion of PB to Prussian white.[25] The scan rate dependency for the voltammetry profile of the PB-TiO_2 antenna NW electrode in the range $50-1000\,mV\,s^{-1}$ is then presented (Figure 4b), in which the electrochemical stability of the PB-TiO_2 antenna NWs is demonstrated by repeating cyclic voltammetry measurements at a scan rate of $50\,mV\,s^{-1}$. There is no observable difference in either current level or peak positions for the cyclic voltammetry curves after 50 cycles (Figure 4c), which confirms the stable structure of the immobilized PB nanocubes on the TiO_2 NW tips.

The capability of using PB-TiO_2 antenna NWs as an amperometric sensing modality for H_2O_2 is further investigated because it is well-known that the reduced form of PB exhibits a high catalytic activity for H_2O_2 reduction.[27] During this process, PB acts as an electron transport mediator between the electrode and H_2O_2 in a solution. The presence of H_2O_2 (5 mM in phosphate buffer saline (PBS), pH of 6.0) leads to a clear increase in current density (corresponding to H_2O_2 reduction) at a lower overpotential (that is, −50 mV versus Ag/AgCl) (Figure 4d). The calculated electron transfer rate constant, k_s, is $5.72 \pm 0.05\,s^{-1}$, which is much greater than that for most of the H_2O_2 electrodes reported previously, such as the ordered nanoporous niobium oxide film ($0.28\,s^{-1}$),[28] NaY zeolite/glassy carbon electrode ($0.78 \pm 0.04\,s^{-1}$)[29] and colloidal Au/carbon paste ($1.21 \pm 0.08\,s^{-1}$).[30]

PB-TiO_2 antenna NW arrays for H_2O_2 sensing

The sensor performance of PB-TiO_2 antenna NWs in detecting H_2O_2 is extensively investigated. Because coexisting molecular interferences, such as AA, O_2 and so on, may affect the electrochemical determination of H_2O_2, the bias potential should be prudently selected to optimize the cathodic current and sensitivity obtained at the PB-TiO_2 antenna NW electrodes. Amperometric experiments were performed to investigate the responses of PB-TiO_2 antennas from H_2O_2 at various potentials of −0.10, −0.05, 0.00, 0.05 and 0.10 V (versus Ag/AgCl). Several interference molecules, which included O_2, Na_2SO_3, uric acid, 3,4-dihydroxyphenylacetic acid, $NaNO_2$ and AA, were tested

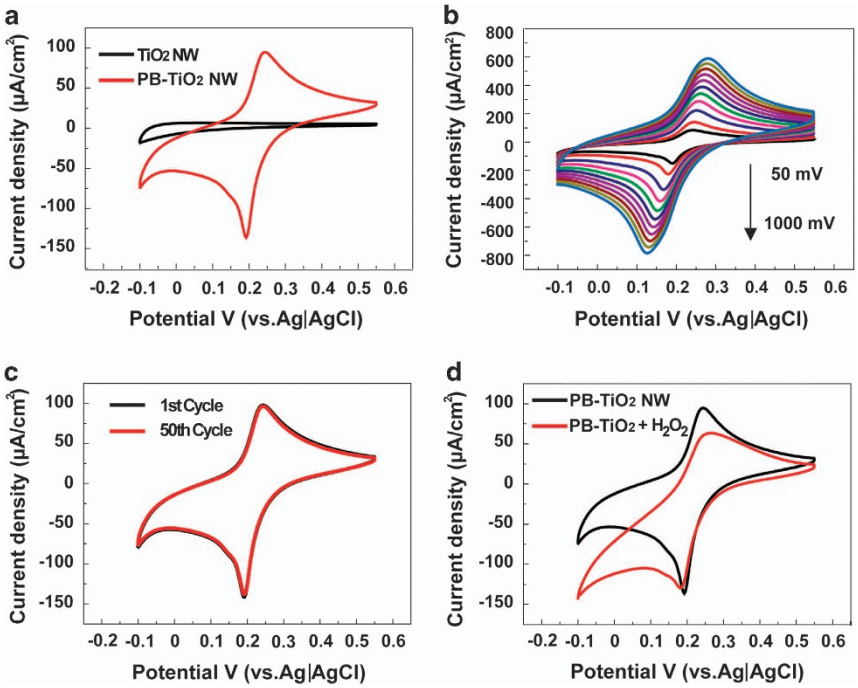

Figure 4 Electrochemical performance of bio-mimetic Prussian blue (PB)-TiO_2 antenna arrays. (**a**) Cyclic voltammograms (CVs) of the blank TiO_2 nanowires (NWs) (black curve) and PB-TiO_2 NWs (red curve) in N_2-saturated 0.05-M phosphate buffer saline (PBS) solution (pH of 6.0) at a scan rate of 50 mV s^{-1}. An Ag/AgCl electrode was used as a reference electrode. (**b**) CVs of PB-TiO_2 NWs in N_2-saturated 0.05-M PBS solution (pH of 6.0) at different scan rates: 50–1000 mV s^{-1} from the inside to the outside. (**c**) The CVs of the first cycle (black curve) and 50th cycle (red curve) of the PB-TiO_2 NWs in the N_2-saturated 0.05-M PBS solution (pH of 6.0) at a scan rate of 50 mV s^{-1}. (**d**) The CVs of a PB-TiO_2 NWs electrode in the N_2-saturated 0.05-M PBS solution (pH of 6.0) in the absence (black curve) and presence of 5 mM H_2O_2 (red curve) at a scan rate of 50 mV s^{-1}.

(Figure 5a). In general, a low anodic current is obtained for the interference molecules at relatively negative potentials. For example, the ratio of anodic current between H_2O_2 to AA (0.1 mM each) increases from 6.8 to 55 A when the applied potential is reduced from 0.10 to −0.05 V (versus Ag/AgCl), which increases the selectivity.[31] Hence, −0.05 V (versus Ag/AgCl) is selected as the optimized operational bias potential. In contrast, control experiments of pristine TiO_2 NWs and TiO_2 NWs post-modified with PB (TiO_2 NWs + PB) do not show a similar high current signal or signal ratios, even at an applied potential of −0.05 V (Figures 5b and c), which suggests that the direct growth and attachment of PB nanocubes on TiO_2 NW tips enhance the sensitivity and selectivity. In addition, these data confirm the bio-mimetic enzymatic amplification nature of the H_2O_2 catalysis at the PB-TiO_2 antenna NW electrodes. The long-term stability of PB-TiO_2 antenna NW electrodes is exemplified by repeating cyclic voltammetry cycles at different bias voltages. The PB-TiO_2 antenna maintains 95% of its initial signal responses, even after 1000 cycles (Figure 5d), which is much more sensitive and stable than pristine TiO_2 NWs and TiO_2 NWs post-modified with PB, which is excellent for long-term signal monitoring (Figures 5e and f).

The amperometric measurement is further investigated by determining the electrocatalytic activity of the PB-TiO_2 antenna NWs for H_2O_2. A substantial cathodic current change is observed at the PB-TiO_2 antenna NW electrodes at −50 mV when 25 μM of H_2O_2 is introduced in the buffer, whereas essentially no response is obtained at the pristine TiO_2 NWs under otherwise similar conditions (Figure 5g). The contribution of the observed anodic current to the catalysis of H_2O_2 is confirmed by adding catalase,[10,32] a selective scavenger of H_2O_2, into the solution with H_2O_2. A large decrease in the cathodic current to essentially the background level is observed, which indicates that the signal response can be ascribed to the catalysis of H_2O_2 by the PB-TiO_2 antenna NW electrodes.

Amperometric responses of the PB-TiO_2 antenna NWs with successive addition of H_2O_2 are conducted at the optimized potential of −50 mV. The stepwise current signal correlates well with each addition of H_2O_2, whereas an almost negligible current response is observed for the pristine TiO_2 NWs (Figure 5h). The calibration plot of the current change obtained at the PB-TiO_2 antenna NWs with the H_2O_2 concentration is summarized (Figure 5i), and the analytical performance of the PB-TiO_2 antenna NW-based H_2O_2 biosensor at the optimum conditions is listed in Supplementary Table S1. Other previously reported H_2O_2 biosensors based on TiO_2 or titanate nanostructures are also listed in Supplementary Table S1 for comparison. The PB-TiO_2 antenna NWs exhibit an excellent sensor performance, which includes their higher selectivity, wider linear detection range and lower detection limit. Specifically, the dynamic linear range of 10^{-8} to 10^{-5} M to detect H_2O_2 at the applied potential of −50 mV is significantly wider than those obtained in previous H_2O_2 biosensing interfaces[33,34] and fulfills the requirement of real-time, long-term tracking of an H_2O_2 concentration (Figure 5i). Moreover, the PB-TiO_2 antenna NW biosensors can be tested and stored at room temperature and can be repeatedly tested for over 180 days without substantial degradation (Supplementary Figure S10), which suggests the high stability of the PB-TiO_2 antenna NW electrodes.

Cell culture and extracellular H_2O_2 sensing

The capability of PB-TiO_2 antenna NW electrodes for direct growth of cells and extracellular H_2O_2 detection is further demonstrated. The uniform coverage of PB nanocubes offers an excellent substrate for

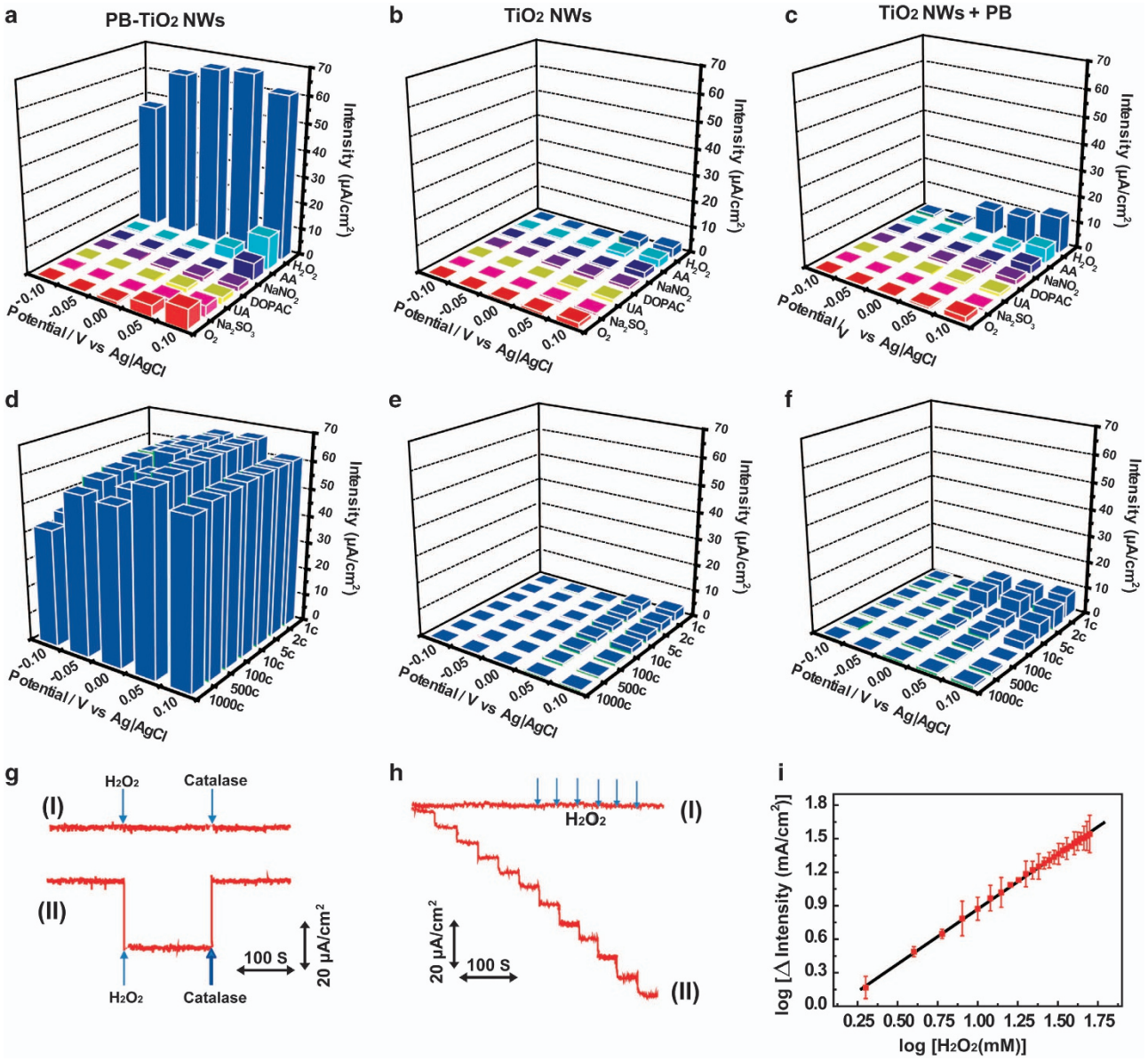

Figure 5 The selectivity, sensitivity, stability and detection range of bio-mimetic Prussian blue (PB)-TiO_2 nanowire (NW) antenna arrays. (**a–c**) The selectivity, sensitivity and (**d–f**) stability profile of the present PB-TiO_2 NW (**a**,**d**) electrodes obtained at different applied potentials: −0.10, −0.05, 0.00, 0.05 and 0.10 V versus Ag/AgCl. The TiO_2 NWs (**b**,**e**) and traditional post-modified PB nanocrystals on TiO_2 NW (**c**,**f**) electrodes were used as control experiments. (**g**) Amperometric responses obtained at the (i) blank TiO_2 NWs and (ii) PB-TiO_2 NWs electrode in 50 mM phosphate buffer saline (PBS) (pH of 6.0) containing 100 mM glucose at the applied potential of 0.0 V versus AgIAgCl with the addition of the final concentration of 25 μM H_2O_2 and 500 U ml^{-1} catalase. (**h**) Typical amperometric responses of (i) blank TiO_2 NWs and (ii) PB-TiO_2 NWs to successive additions of 10 μM H_2O_2 at an applied potential of −0.05 V versus AgIAgCl in 50 mM PBS (pH of 6.0). (**i**) Log-response curve of steady-state currents obtained at the PB-TiO_2 NW electrode against concentrations of H_2O_2.

cell attachment and growth, which can subsequently produce H_2O_2 via different cell functions (Figure 6a).[35–37] The fluorescence images of HeLa cells grown on top of the PB-TiO_2 antenna NWs clearly confirm a good coverage of cells on the NWs (Figure 6b). The cell viability is measured by [3-(4,5-dimethylthiazol-2-yl)-2,5-diphenyltetrazolium bromide] (MTT) in a Nun Immune Omni Tray (Angle Nun International, Rochester, NY, USA; Experimental Section in Supporting Information, Supplementary Figures S11–S13), which shows that a high HeLa cell viability (>80%) is maintained for growth for up to 5 h (Figure 6c). The measured amperometric responses obtained at the bio-interface between the PB-TiO_2 antenna NWs and HeLa cells are 50 mM PBS (pH of 6.0) at an applied potential of −50 mV versus Ag|AgCl (Figure 6c). When 50 mM of PMA is injected into the HeLa cell-NW assay, an increase in the cathodic current is observed (Figure 6d). This phenomenon is attributed to the effect of PMA for inducing H_2O_2 production from the cells.[10] An anodic current increase of ~32.5 μA is obtained in 15 s, which is similar to the time scale reported previously.[38] No response is observed at the bare TiO_2 NWs with the same addition of PMA. In addition, the injection of the catalase solution (300 U ml^{-1} in PBS) reduces the current level to almost the background current level; catalase is known to inhibit the PMA function.[10] Accordingly,

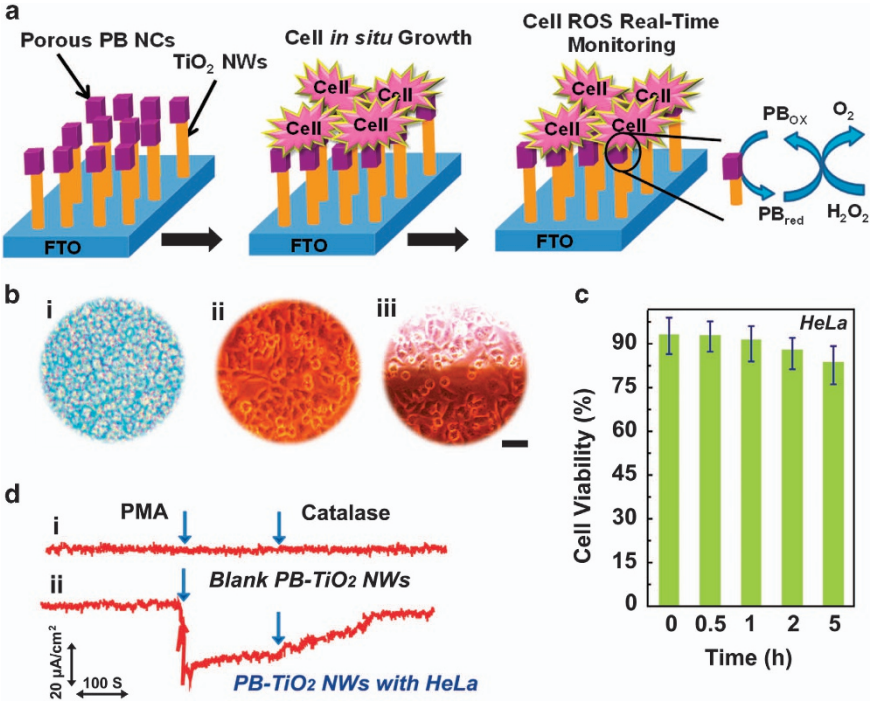

Figure 6 Ultra-sensitive bio-interface based on bio-mimetic antenna Prussian blue (PB)-TiO_2 nanowire (NW) arrays. (**a**) Schematic illustration of the PB-TiO_2 NW arrays bio-interface for *in-situ* living cell culture and real-time three-dimensional recognition and biosensing. (**b**) Fluorescence microscopic images of (i) PB-TiO_2 NWs, (ii) PB-TiO_2 NWs with *in situ*-cultured Hela cells, and (iii) the interface of PB-TiO_2 NWs and culture dish with *in situ*-cultured Hela cells (12 h). The scale bar is 50 μm for (i–iii). (**c**) Cell viability of cells cultured on PB-TiO_2 NWs with the amount of testing time. (**d**) Amperometric responses obtained at the (i) blank PB-TiO_2 NWs and (ii) PB-TiO_2 NWs with HeLa cell incubation. The measurement was performed in 50 mM phosphate buffer saline (pH of 6.0) that contained 100 mM glucose at the applied potential of −0.05 V versus Ag/AgCl after the final injection concentrations of 50 mM Phorbol 12-myristate-3-acetate (PMA) and 300 U ml^{-1} catalase.

the increase in cathodic current at the PB-TiO_2 antenna NW bio-interface located near the cells is ascribed to the enzymatic reduction of H_2O_2, which is effectively mediated by the PB nanocubes grown on the TiO_2 NWs interface.

The much enhanced sensitivity of the bio-mimetic PB-TiO_2 antenna NWs is attributed to the unique bio-inspired head/arm heterostructure, in which intimate contact between the PB nanocube heads and the TiO_2 NW arms can create synergistic properties of both components. The porous PB nanocubes offer a robust substrate for site-selective cell adhesion and cultivation of living cells because the porous nanocubes exhibit high selectivity and bioaffinity toward cells and have excellent biostability under the cell culture adhesion condition (up to 108 h) (Supplementary Figure S14). Furthermore, the porous nanocrystals can also serve as long-term stable and sensitive sensing elements for H_2O_2 due to their inherent bio-mimetic enzymatic activity, high surface area and 3D stereo space-based signal molecules for touching and recognition. In addition, compared with conventional planar PB-covered electrochemical interfaces,[39,40] the electrocatalytic activity is enhanced at the PB-TiO_2 antenna NW biointerfaces due to the rapid charge transport realized by the one-dimensional TiO_2 NW structure. Thus, this PB-TiO_2 antenna NW demonstrates a new sensing platform to reliably and durably detect extracellular molecules.

CONCLUSIONS

In summary, a bio-mimetic PB-TiO_2 antenna NW array-based bio-interface is demonstrated for the first time as an excellent structure that can recognize 3D signal molecules and that can be used for biosensing. Living cell adhesion and *in-situ* cultivation on PB-TiO_2 antennas, which integrates with sensitive real-time monitoring of cellular messenger molecules, are realized by the dual-functional PB nanocube heads and TiO_2 NW arms. The optimized PB-TiO_2 antenna NW biointerfaces exhibit a remarkable sensing performance in detecting H_2O_2 with a high sensitivity and selectivity, a broad detection range from 10^{-8} to 10^{-5} M, a low detection limit down to 20 nM and a short response time that is within 5 s. In addition, bio-mimetic PB nanocrystals are stably anchored on the TiO_2 NWs and can maintain long-term biocatalytic activity (up to ~180 days). The capability of the PB-TiO_2 antenna NW biointerfaces in determining extracellular H_2O_2 released from human tumor cells is further demonstrated. This work not only provides a method for 3D interface recognition and biosensing on the hierarchical bio-mimetic nanostructured semiconductors but also suggests a general approach for durable, reliable biomolecule detection in biological systems.

CONFLICT OF INTEREST

The authors declare no conflict of interest.

ACKNOWLEDGEMENTS

We thank the following funding agencies for supporting this work: the National Key Basic Research Program of China (2013CB934104, 2012CB224805), the NSF of China (20890123, 21322311, and 21071033), the Program for New Century Excellent Talents in University (NCET-10-0357), the Program for Professor of Special Appointment (Eastern Scholar) at the Shanghai Institutions of Higher Learning and the Deanship of Scientific Research of the King Saud University (IHCRG#14-102) and the Shanghai Science and Technology Municipality (14JC1490500). BK and JT thank the

Scholarship Award for Excellent Doctoral Student granted by the Ministry of Education of China and the Interdisciplinary Outstanding Doctoral Research Funding of the Fudan University.

1 Schutz, S., Weissbecker, B., Hummel, H. E., Apel, K.-H., Schmitz, H. & Bleckmann, H. Insect antenna as a smoke detector. *Nature* **398,** 298–299 (1999).
2 Cayirlioglu, P., Kadow, I. G., Zhan, X., Okamura, K., Suh, G. S., Gunning, D., Lai, E. C. & Zipursky, S. L. Hybrid neurons in a microRNA mutant are putative evolutionary intermediates in insect CO_2 sensory systems. *Science* **319,** 1256–1260 (2008).
3 Pruneanu, S., Pogacean, F., Biris, A. R., Ardelean, S., Canpean, V., Blanita, G., Dervishi, E. & Biris, A. S. Novel graphene-gold nanoparticle modified electrodes for the high sensitivity electrochemical spectroscopy detection and analysis of carbamazepine. *J. Phys. Chem. C* **115,** 23387–23394 (2011).
4 Eu, J. P., Sun, J., Xu, L., Stamler, J. S. & Meissner, G. The skeletal muscle calcium release channel: coupled O_2 sensor and NO signaling functions. *Cell* **102,** 499–509 (2000).
5 Flavahan, W. A., Wu, Q., Hitomi, M., Rahim, N., Kim, Y., Sloan, A. E., Weil, R. J., Nakano, I., Sarkaria, J. N. & Stringer, B. W. Brain tumor initiating cells adapt to restricted nutrition through preferential glucose uptake. *Nat. Neurosci.* **16,** 1373–1382 (2013).
6 Morgan, B., Ezeriņa, D., Amoako, T. N., Riemer, J., Seedorf, M. & Dick, T. P. Multiple glutathione disulfide removal pathways mediate cytosolic redox homeostasis. *Nat. Chem. Biol.* **9,** 119–125 (2012).
7 Zhou, S., Narukami, T., Masuo, S., Shimizu, M., Fujita, T., Doi, Y., Kamimura, Y. & Takaya, N. NO-inducible nitrosothionein mediates NO removal in tandem with thioredoxin. *Nat. Chem. Biol.* **9,** 657–663 (2013).
8 Otterbein, L. E., Bach, F. H., Alam, J., Soares, M., Lu, H. T., Wysk, M., Davis, R. J., Flavell, R. A. & Choi, A. M. Carbon monoxide has anti-inflammatory effects involving the mitogen-activated protein kinase pathway. *Nat. Med.* **6,** 422–428 (2000).
9 Lin, V. S., Lippert, A. R. & Chang, C. J. Cell-trappable fluorescent probes for endogenous hydrogen sulfide signaling and imaging H_2O_2-dependent H_2S production. *Proc. Natl Acad. Sci. USA* **110,** 7131–7135 (2013).
10 Luo, Y., Liu, H., Rui, Q. & Tian, Y. Detection of extracellular H_2O_2 released from human liver cancer cells based on TiO_2 nanoneedles with enhanced electron transfer of cytochrome c. *Anal. Chem.* **81,** 3035–3041 (2009).
11 Ferlay, S., Mallah, T., Ouahes, R., Veillet, P. & Verdaguer, M. A room-temperature organometallic magnet based on Prussian blue. *Nature* **378,** 701–703 (1995).
12 Li, J., Li, Y., Zhang, Y. & Wei, G. Highly sensitive molecularly imprinted electrochemical sensor based on the double amplification by an inorganic prussian blue catalytic polymer and the enzymatic effect of glucose oxidase. *Anal. Chem.* **84,** 1888–1893 (2012).
13 Nossol, E. & Zarbin, A. J. A simple and innovative route to prepare a novel carbon nanotube/prussian blue electrode and its utilization as a highly sensitive H_2O_2 amperometric sensor. *Adv. Funct. Mat.* **19,** 3980–3986 (2009).
14 Zhu, A., Luo, Y. & Tian, Y. Plasmon-induced enhancement in analytical performance based on gold nanoparticles deposited on TiO_2 film. *Anal. Chem.* **81,** 7243–7247 (2009).
15 Baker, M. Tissue models: a living system on a chip. *Nature* **471,** 661–665 (2011).
16 Schwille, P. Bottom-up synthetic biology: engineering in a Tinkerer's world. *Science* **333,** 1252–1254 (2011).
17 Liu, X., Chen, L., Liu, H., Yang, G., Zhang, P., Han, D., Wang, S. & Jiang, L. Bio-inspired soft polystyrene nanotube substrate for rapid and highly efficient breast cancer-cell capture. *Asia Mat.* **5,** e63 (2013).
18 Tian, B., Liu, J., Dvir, T., Jin, L., Tsui, J. H., Qing, Q., Suo, Z., Langer, R., Kohane, D. S. & Lieber, C. M. Macroporous nanowire nanoelectronic scaffolds for synthetic tissues. *Nat. Mater.* **11,** 986–994 (2012).
19 Kim, D.-H., Lu, N., Ghaffari, R. & Rogers, J. A. Inorganic semiconductor nanomaterials for flexible and stretchable bio-integrated electronics. *Asia Mat.* **4,** e15 (2012).
20 Hochbaum, A. I. & Yang, P. Semiconductor nanowires for energy conversion. *Chem. Rev.* **110,** 527–546 (2009).
21 Solanki, P. R., Kaushik, A., Agrawal, V. V. & Malhotra, B. D. Nanostructured metal oxide-based biosensors. *Asia Mat.* **3,** 17–24 (2011).
22 Xu, M., Da, P., Wu, H., Zhao, D. & Zheng, G. Controlled Sn-doping in TiO_2 nanowire photoanodes with enhanced photoelectrochemical conversion. *Nano. Lett.* **12,** 1503–1508 (2012).
23 Tang, J., Kong, B., Wang, Y., Xu, M., Wang, Y., Wu, H. & Zheng, G. Photoelectrochemical detection of glutathione by IrO_2–Hemin–TiO_2 nanowire arrays. *Nano. Lett.* **13,** 5350–5354 (2013).
24 Guo, W., Xu, C., Wang, X., Wang, S., Pan, C., Lin, C. & Wang, Z. L. Rectangular bunched rutile TiO_2 nanorod arrays grown on carbon fiber for dye-sensitized solar cells. *J. Am. Chem. Soc.* **134,** 4437–4441 (2012).
25 Wang, T., Fu, Y., Bu, L., Qin, C., Meng, Y., Chen, C., Ma, M., Xie, Q. & Yao, S. Facile synthesis of prussian blue-filled multiwalled carbon nanotubes nanocomposites: exploring filling/electrochemistry/mass-transfer in nanochannels and cooperative biosensing mode. *J. Phys. Chem. C* **116,** 20908–20917 (2012).
26 Zhang, X.-Q., Gong, S.-W., Zhang, Y., Yang, T., Wang, C.-Y. & Gu, N. Prussian blue modified iron oxide magnetic nanoparticles and their high peroxidase-like activity. *J. Mat. Chem.* **20,** 5110–5116 (2010).
27 Song, Y.-Y., Jia, W. Z., Li, Y., Xia, X. H., Wang, Q. J., Zhao, J. W. & Yan, Y. D. Synthesis and patterning of prussian blue nanostructures on silicon wafer via galvanic displacement reaction. *Adv. Funct. Mat.* **17,** 2808–2814 (2007).
28 Zhao, J., Zhu, X., Li, T. & Li, G. Self-assembled multilayer of gold nanoparticles for amplified electrochemical detection of cytochrome c. *Analyst* **133,** 1242–1245 (2008).
29 Dai, Z., Liu, S. & Ju, H. Direct electron transfer of cytochrome *c* immobilized on a NaY zeolite matrix and its application in biosensing. *Electrochim. Acta.* **49,** 2139–2144 (2004).
30 Ju, H., Liu, S., Ge, B., Lisdat, F. & Scheller, F. W. Electrochemistry of cytochrome *c* immobilized on colloidal gold modified carbon paste electrodes and its electrocatalytic activity. *Electroanalysis* **14,** 141–147 (2002).
31 Li, X., Liu, Y., Zhu, A., Luo, Y., Deng, Z. & Tian, Y. Real-time electrochemical monitoring of cellular H_2O_2 integrated with in situ selective cultivation of living cells based on dual functional protein microarrays at Au-TiO_2 surfaces. *Anal. Chem.* **82,** 6512–6518 (2010).
32 Mesquita, A., Weinberger, M., Silva, A., Sampaio-Marques, B., Almeida, B., Leão, C., Costa, V., Rodrigues, F., Burhans, W. C. & Ludovico, P. Caloric restriction or catalase inactivation extends yeast chronological lifespan by inducing H_2O_2 and superoxide dismutase activity. *Proc. Natl Acad. Sci. USA* **107,** 15123–15128 (2010).
33 Liu, H., Tian, Y. & Xia, P. Pyramidal, rodlike, spherical gold nanostructures for direct electron transfer of copper, zinc-superoxide dismutase: application to superoxide anion biosensors. *Langmuir* **24,** 6359–6366 (2008).
34 Zhang, L., Zhang, Q. & Li, J. Layered titanate nanosheets intercalated with myoglobin for direct electrochemistry. *Adv. Funct. Mat.* **17,** 1958–1965 (2007).
35 Root, R. K. & Metcalf, J. A. H_2O_2 release from human granulocytes during phagocytosis: relationship to superoxide anion formation and cellular catabolism of H_2O_2: studies with normal and cytochalasin B-treated cells. *J. Clin. Invest.* **60,** 1266 (1977).
36 Wang, D., Youngson, C., Wong, V., Yeger, H., Dinauer, M. C., De Miera, E. V.-S., Rudy, B. & Cutz, E. NADPH-oxidase and a hydrogen peroxide-sensitive K^+ channel may function as an oxygen sensor complex in airway chemoreceptors and small cell lung carcinoma cell lines. *Proc. Natl Acad. Sci. USA* **93,** 13182–13187 (1996).
37 Pei, Z.-M., Murata, Y., Benning, G., Thomine, S., Klüsener, B., Allen, G. J., Grill, E. & Schroeder, J. I. Calcium channels activated by hydrogen peroxide mediate abscisic acid signalling in guard cells. *Nature* **406,** 731–734 (2000).
38 Zhu, A., Tian, Y., Liu, H. & Luo, Y. Nanoporous gold film encapsulating cytochrome *c* for the fabrication of a H_2O_2 biosensor. *Biomaterials* **30,** 3183–3188 (2009).
39 Karyakin, A. A., Karyakina, E. E. & Gorton, L. Amperometric biosensor for glutamate using Prussian blue-based 'artificial peroxidase' as a transducer for hydrogen peroxide. *Anal. Chem.* **72,** 1720–1723 (2000).
40 Moscone, D., D'ottavi, D., Compagnone, D., Palleschi, G. & Amine, A. Construction and analytical characterization of Prussian blue-based carbon paste electrodes and their assembly as oxidase enzyme sensors. *Anal. Chem.* **73,** 2529–2535 (2001).

Supplementary Information accompanies the paper on the website (http://www.nature.com/am)